Proton Radiography of Inertial Fusion Implosions
J. R. Rygg, *et al.*
Science **319**, 1223 (2008);
DOI: 10.1126/science.1152640

11. S. G. Moiseenko, G. S. Bisnovatyi-Kogan, N. V. Ardeljan, *Mon. Not. R. Astron. Soc.* **370**, 501 (2006).
12. D. C. Leonard *et al.*, *Nature* **440**, 505 (2006).
13. L. Wang, D. A. Howell, P. Höflich, J. C. Wheeler, *Astrophys. J.* **550**, 1030 (2001).
14. K. S. Kawabata *et al.*, *Astrophys. J.* **580**, L39 (2002).
15. D. C. Leonard, A. V. Filippenko, R. Chornock, R. J. Foley, *Pub. Astron. Soc. Pac.* **114**, 1333 (2002).
16. L. Wang, D. Baade, P. Höflich, J. C. Wheeler, *Astrophys. J.* **592**, 457 (2003).
17. K. Maeda *et al.*, *Astrophys. J.* **565**, 405 (2002).
18. P. A. Mazzali *et al.*, *Science* **308**, 1284 (2005).
19. A. M. Soderberg, E. Nakar, E. Berger, S. R. Kulkarni, *Astrophys. J.* **638**, 930 (2006).
20. N. Kashikawa *et al.*, *Pub. Astron. Soc. Jpn.* **54**, 819 (2002).
21. T. Matheson, A. V. Filippenko, W. Li, D. C. Leonard, J. C. Shields, *Astron. J.* **121**, 1648 (2001).
22. Data and methods are available as supporting material on *Science* Online.
23. K. Maeda, K. Nomoto, P. A. Mazzali, J. Deng, *Astrophys. J.* **640**, 854 (2006).
24. K. Maeda, K. Nomoto, *Astrophys. J.* **598**, 1163 (2003).
25. A. M. Khokhlov *et al.*, *Astrophys. J.* **524**, L107 (1999).
26. A. I. MacFadyen, S. E. Woosley, A. Heger, *Astrophys. J.* **550**, 410 (2001).
27. K. Maeda, P. A. Mazzali, K. Nomoto, *Astrophys. J.* **645**, 1331 (2006).
28. M. Modjaz *et al.*, *Astron. J.*, http://arxiv.org/abs/astro-ph/0701246 (2007).
29. A. I. MacFadyen, S. E. Woosley, *Astrophys. J.* **524**, 262 (1999).
30. H. A. Bethe, J. R. Wilson, *Astrophys. J.* **295**, 14 (1985).
31. M. Modjaz, R. P. Kirshner, P. Challis, preprint available at http://arxiv.org/abs/0801.0221 (2008).
32. The data were collected at the NAOJ Subaru telescope. The additional data were from the ESO VLT under ESO program 078.D-0246. K.M. and M.T. have been supported by the Japan Society for the Promotion of Science (JSPS). E.P. and P.M. acknowledge financial support from PRIN MUIR 2005 and PRIN INAF 2006. K.N. is supported by a JSPS Grant-in-Aid for Scientific Research (18104003 and 18540231). J.D. is supported by the National Natural Science Foundation of China (grant no. 10673014). A.V.F. is supported by NSF grant AST-0607485.

Proton Radiography of Inertial Fusion Implosions

J. R. Rygg,[1]* F. H. Séguin,[1] C. K. Li,[1] J. A. Frenje,[1] M. J.-E. Manuel,[1] R. D. Petrasso,[1]† R. Betti,[2] J. A. Delettrez,[2] O. V. Gotchev,[2] J. P. Knauer,[2] D. D. Meyerhofer,[2] F. J. Marshall,[2] C. Stoeckl,[2] W. Theobald[2]

A distinctive way of quantitatively imaging inertial fusion implosions has resulted in the characterization of two different types of electromagnetic configurations and in the measurement of the temporal evolution of capsule size and areal density. Radiography with a pulsed, monoenergetic, isotropic proton source reveals field structures through deflection of proton trajectories, and areal densities are quantified through the energy lost by protons while traversing the plasma. The two field structures consist of (i) many radial filaments with complex striations and bifurcations, permeating the entire field of view, of magnetic field magnitude 60 tesla and (ii) a coherent, centrally directed electric field of order 10^9 volts per meter, seen in proximity to the capsule surface. Although the mechanism for generating these fields is unclear, their effect on implosion dynamics is potentially consequential.

Identification and characterization of the physical phenomena associated with dynamic, extreme states of matter—such as those of high–energy-density physics (*1*, *2*) found in inertial fusion (*3*, *4*), laboratory astrophysics (*2*, *5*), and laser-plasma interaction physics (*6*)—are of fundamental scientific importance. A novel method of diagnosing inertial fusion implosions has resulted in the characterization of two distinct electromagnetic field configurations that have potentially consequential effects on implosion dynamics. This method also makes possible the quantitative study of the temporal evolution of capsule size and areal density.

The method involves radiography with a pulsed (0.1 ns), monoenergetic (15.0 MeV), quasi-isotropic proton source (*7*, *8*). Fields are revealed in radiographs through deflection of proton trajectories, and areal densities are quantified through the energy lost by protons while traversing the plasma. The imaged samples are inertial confinement fusion (ICF) capsules of the fast-ignition (FI) variety (*9*, *10*), initially 430 µm in radius, imploded by 36 laser beams that deposit 14 kJ of energy in a 1-ns pulse (*8*).

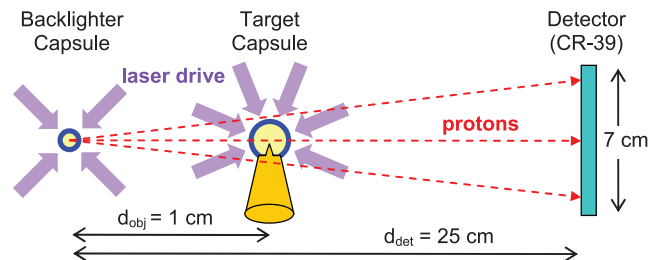For electricity generation (*3*, *4*) and for studies of extremely high–energy-density physics (*1*, *2*) in the laboratory, ICF seeks to release copious energy by igniting a compressed pellet of fusion fuel. Fuel compression to densities of 300 g/cm^3 or higher will be achieved by energy deposition onto the surface of a fuel capsule over nanosecond time scales, either by laser light (direct drive) or by x-rays generated in a cavity by laser light (indirect drive). Ignition and energy gain will occur in a central hot spot, or, in the FI scheme, by the extremely rapid (picosecond-scale) deposition of additional energy, either directly onto the compressed pellet (*9*) or along the axis of a cone that keeps the path clear of plasma ablated from the pellet surface (*10*).

The 15-MeV (fig. S1), monoenergetic proton radiography applied herein was recently used by Li *et al.* in a different context to investigate fields generated by laser-foil interactions (*11*, *12*). Mackinnon *et al.* (*13*) used a broad-band, non-isotropic proton source to study six-beam implosions, though they did not observe either striated or coherent field structures. In addition, earlier workers, using optical techniques largely sensitive to density perturbations, observed very-fine-scale radial filaments and jets (*14*, *15*) in targets driven by one to four laser beams. However, the character of these structures is qualitatively different in several ways from the striations described in this report [see supporting online material (SOM) text].

In the reported experiments (Fig. 1), cone-in-shell FI targets were radiographed before and during implosion, 1.56 ns after the start of the

[1]Plasma Science and Fusion Center, Massachusetts Institute of Technology, Cambridge, MA 02139, USA. [2]Laboratory for Laser Energetics, University of Rochester, Rochester, NY 14623, USA.

*Present address: Lawrence Livermore National Laboratory, Livermore, CA 94551, USA.
†To whom correspondence should be addressed. E-mail: petrasso@psfc.mit.edu

Fig. 1. Schematic of the experimental setup. A short (130-ps), monoenergetic (energy linewidth $\Delta E/E <$ 3%), quasi-isotropic pulse of 15.0-MeV D^{3}He fusion protons is generated by laser implosion of a backlighter capsule filled with D$_2$ and ^{3}He gas. The $\sim 3 \times 10^8$ protons emitted from the 45-µm full width at half maximum source region interact with matter and electromagnetic fields in a cone-in-shell capsule implosion. The position and energy of every proton reaching the detector are individually recorded on CR-39, encoding the details of the matter and field distributions surrounding the target capsule.

laser drive (Fig. 2), shortly after the end of the acceleration phase (4). The radiographs were taken perpendicular to the Au cone axis. Figure 3 shows the experimental results (which are also characteristic of many implosions without cones). Because the detector records proton fluence and energy, Fig. 3 shows images illustrating the spatial distributions of both proton fluence and mean proton energy.
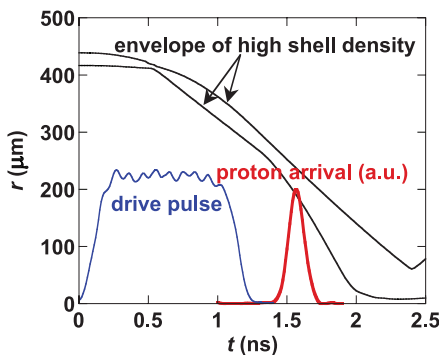
Five important features are apparent in these images. First, the character of the isotropic and monoenergetic proton source is reflected in the uniform background of Fig. 3, A and C. Second, a complex filamentary structure is seen in the fluence image of Fig. 3B. The uniform energy seen outside the capsule in Fig. 3D demonstrates that the fluence striations are due to electromagnetic deflection rather than to scattering through plasma density filaments. Third, substantial plasma blowoff from the cone casts a much wider shadow as the capsule is imploded. Fourth, a significant enhancement of the proton fluence at the center of the imploded target (Fig. 3B) suggests the presence of a radially directed, focusing electric field. Finally, radial compression of the capsule by a factor of two is seen in Fig. 3D. The basic repeatability of the field structure and capsule compression was demonstrated by radiographs taken at the same relative time but on different implosions.

In the radiographic images, field structure is studied by means of the spatial distribution of proton fluence. The proton-path–integrated electric (E) or magnetic (B) field can be estimated from the angular deflection θ of protons of energy E_p passing through the field region:

$$\int E_\perp dl = 2(E_p/e)\tan\theta \qquad (1)$$

$$\int B \times dl = (m_p v_p/e)\sin\theta \qquad (2)$$

$$\tan\theta = M\xi/(d_{det} - d_{obj}) \qquad (3)$$

where m_p is the proton mass, v_p is the proton speed, e is the fundamental unit charge, the magnification $M = 25$, and d_{det} and d_{obj} are the distances from the backlighter capsule to the detector and to the target capsule, respectively (Fig. 1). The deflection angle is determined by measuring the apparent displacement ξ of protons in the target plane via Eq. 3.
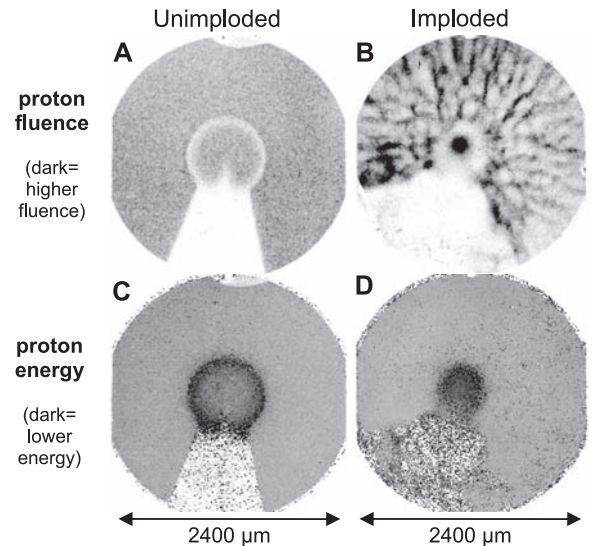
Areal density at different positions in the target capsule is studied through the downshift in proton energy relative to the incident energy of 15.0 MeV. It is proportional to the amount of matter traversed between the source and detector (16), quantified by ρL ($= \int \rho dl$).

Radial lineouts of the images in Fig. 3 are shown in Fig. 4. In the fluence lineout for the imploded target (Fig. 4B), the value near radius $r = 0$ μm is markedly enhanced relative to the values at large radii (by a factor of three) and at $r = 200$ μm (by a factor of six). To explain this

result, we found that a radial electric field of about 1.5×10^9 V/m is necessary to "focus" 15.0-MeV protons, to the extent observed, passing near $r = 200$ μm toward the center. Scattering is insufficient to explain this result (fig. S4).

We conjecture that this coherent field is a consequence of a large, outward-directed electron pressure gradient that exists in the vicinity of the fuel-shell interface. Such a field might be expected to occur during, and shortly after, the acceleration phase of the implosion in which substantial shell mass is rapidly assembled and compressed. Such an electric field—given by $-\nabla P_e/en_e$, where P_e and n_e are the electron pressure and density—has been observed in the context of other recent laser plasma experiments (11). If this conjecture is correct, future measurements of the evolution of this coherent E field might effectively map capsule pressure dynamics throughout the implosion. Such information

Fig. 3. Images of a 430-μm-radius spherical plastic capsule with attached Au cone, before and during implosion. (**A** and **C**) The unimploded capsule used in OMEGA shot 46531. (**B** and **D**) A capsule at 1.56 ns after the onset of the laser drive (OMEGA shot 46529). The dark areas correspond to regions of higher proton fluence [in (A) and (B)] and regions of lower proton energy [in (C) and (D)]. The energy image values in the region shadowed by the cone are mostly noise because very few protons were detected in that region. See lineouts in Figs. 4 and 5 for image values.

Fig. 2. Cone-in-shell capsule drive pulse (blue line), simulated (17) shell trajectory (black lines), and experimental backlighter proton arrival time t (red line). Simulations predict that the shell has compressed from its original radius by about a factor of two, and the ρR has doubled to 5 mg/cm² when the backlighter protons arrive at 1.56 ns (OMEGA shot 46529). a.u., arbitrary units.

Fig. 4. Experimental (exp.) radial lineouts (red lines) of proton fluence and ρL from Fig. 3. All lineouts are averaged over the azimuth, excluding the region of the cone shadow. (**A** and **C**) Unimploded capsule of OMEGA shot 46531. (**B** and **D**) Capsule of OMEGA shot 46529, 1.56 ns after start of laser drive. The fluence lineout (A) shows the effects of angular scattering through the limb of the capsule shell. In (B), angular scattering effects alone are insufficient to explain the peak at $r = 0$. A radial electric field of ~10^9 V/m is necessary to focus the protons to the extent observed. In (C) and (D), radial lineouts of the mean energy images in Fig. 3 were converted to ρL. Also displayed are the actual ρL (C) and simulated ρL (D), assuming no angular scattering (black line). ρR is given by $\rho L/2$ at $r = 0$.
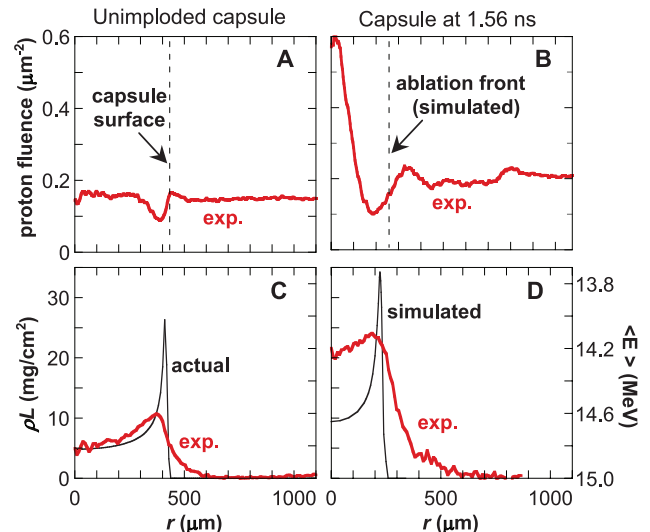
would be invaluable in assessing implosion performance.

Lineouts of the mean energy images of Fig. 3, C and D, can be used to infer the mean path areal density ρL, shown in Fig. 4, C and D. The ρL lineout of the unimploded target (Fig. 4C) gives an initial radial areal density (ρR) of 2.5 mg/cm^2, which is very close to the actual initial ρR of 2.4 mg/cm^2. Scattering of protons smears out measured ρL values near the limb of the shell at $r = 410$ μm. Both measurement and simulation (17) indicate a factor of two reduction in capsule radius at 1.56 ns. However, the ρL lineout of the imploded capsule at 1.56 ns (Fig. 4D) implies that the capsule ρR has increased to 10 mg/cm^2, which is twice the 5 mg/cm^2 predicted by numerical simulation. This high apparent experimental ρR is due in part to scattering and in part to E-field focusing of the lower-energy protons passing through the limb of the capsule shell.

Returning to the filamentary fields, we note how the outer edge of the coherent field merges, at a boundary just outside the imploding capsule, into the striated fields. As illustrated in Fig. 5C and fig. S3, the striated fields originate inside the critical surface, which is extremely close to the capsule surface. Azimuthal lineouts of the proton fluence image of Fig. 3B at radii 430 and 860 μm show the amplitude and scale of proton fluence variations (Fig. 5) due to striations. Peak-to-valley fluence modulations of a factor of four are seen at both radii. The typical angular oscillation period is 20° and 10° for the inner and outer radii, respectively, corresponding to the same spatial distance between striations of 150 μm. This distance implies a deflection angle of 0.45°, which gives a path-integrated magnetic field $\int B \times dl$ of 4000 T·μm. Assuming an integration path length equal to the typical width of striations (75 μm) results in a magnetic field strength of ~60 T. If the fluence variations are instead due to E fields, the field strength required is ~3×10^9 V/m, although quasi-neutrality of the coronal plasma with no laser energy source makes this interpretation unlikely.

The occurrence of such strong inhomogeneities inside the critical surface ~0.5 ns after the laser drive ends suggests that substantially larger fields are likely present just before laser

shutoff (18, 19). This situation would be reflected in a Hall parameter ($\omega\tau$) of order 1 or larger, the inverse square of which reduces the classical electron heat transport (18, 19). This situation would result in the inhomogeneous inhibition of thermal transport over the capsule surface, altering even the zeroth-order hydrodynamics (19, 20). Whether the source of these inhomogeneities is Rayleigh-Taylor (RT) (21), electrothermal (20), collisional Weibel (14, 18), or another instability, they could provide seeds for RT growth, which, if too substantial, could degrade capsule compression and quench ignition during final stagnation phase (4, 18, 19). These issues are being actively investigated.

It seems plausible that either the electrothermal or RT instability could be the relevant source. Ongoing planar experiments, in which RT was purposely seeded, measured B fields of order 100 T with the use of the monoenergetic particle methods described here (see SOM text). Furthermore, estimates [based on (19)] of the RT-generated B field under similar conditions give fields of the same magnitude (see SOM text). Radiography of driven solid plastic capsules, which undergo no acceleration to drive RT growth, could be used to determine whether RT is a contributing mechanism.

Finally, the vast spatial extent of these striated fields likely reflects their outward convection resulting from the plasma flow, because the fields are tied to the outflowing plasma resulting from high plasma electrical conductivity. We conjecture that these radiographic images thus provide snapshots of filamentary structures originally produced inside the critical surface at various times during the implosion.

Two distinctly different, simultaneously occurring electromagnetic field structures, with important implications for implosion dynamics, have been characterized in imploding ICF capsules. First, a complex filamentary field topology permeates the entire 2400-μm field of view with striations corresponding to 60-T magnetic fields. This field, through the inhomogeneous inhibition of heat flux in the vicinity of the ablation surface, could generate seeds for RT growth,

thereby affecting the overall implosion dynamics (4, 6, 19, 20). Second, a coherent, radial electric field of magnitude 10^9 V/m exists in the immediate vicinity of the capsule, dramatically focusing protons toward the center (22). This hitherto-unobserved field is conjectured to originate from the gradient of electron pressure. If verified, a window for analyzing the evolution of the internal pressure dynamics is opened; this would be of immense value for critically assessing the entire implosion process.

References and Notes

1. National Research Council, *Frontiers in High Energy Density Physics* (National Academies Press, Washington, DC, 2003).
2. R. P. Drake, *High-Energy-Density Physics* (Springer, New York, 2006).
3. J. Nuckolls, L. Wood, A. Thiessen, G. Zimmerman, *Nature* **239**, 139 (1972).
4. S. Atzeni, J. Meyer-ter-Vehn, *The Physics of Inertial Fusion* (Oxford Univ. Press, New York, 2004).
5. B. A. Remington, R. P. Drake, D. D. Ryutov, *Rev. Mod. Phys.* **78**, 755 (2006).
6. W. L. Kruer, *The Physics of Laser Plasma Interactions* (Westview, Boulder, CO, 2003).
7. C. K. Li *et al.*, *Rev. Sci. Instrum.* **77**, 10E725 (2006).
8. Materials and methods are available as supporting material on *Science* Online.
9. M. Tabak *et al.*, *Phys. Plasmas* **1**, 1626 (1994).
10. R. Kodama *et al.*, *Nature* **418**, 933 (2002).
11. C. K. Li *et al.*, *Phys. Rev. Lett.* **97**, 135003 (2006).
12. C. K. Li *et al.*, *Phys. Rev. Lett.* **99**, 055001 (2007).
13. A. J. Mackinnon *et al.*, *Phys. Rev. Lett.* **97**, 045001 (2006).
14. T. Mochizuki *et al.*, *Jpn. J. Appl. Phys.* **19**, L645 (1980).
15. O. Willi, P. T. Rumsby, *Opt. Commun.* **37**, 45 (1981).
16. C. K. Li, R. D. Petrasso, *Phys. Rev. Lett.* **70**, 3059 (1993).
17. Numerical simulations of full-sphere capsules, equivalent to the target capsule with no cone, were performed with the one-dimensional (1D) hydrodynamic code LILAC (23). The use of 1D spherical geometry to simulate the areal density of cone-in-shell capsules was previously used and found reasonable (24).
18. M. G. Haines, *Can. J. Phys.* **64**, 912 (1986).
19. A. Nishiguchi, *Jpn. J. Appl. Phys.* **41**, 326 (2002).
20. M. G. Haines, *Phys. Rev. Lett.* **47**, 917 (1981).
21. K. Mima, T. Tajima, J. N. Leboeuf, *Phys. Rev. Lett.* **41**, 1715 (1978).
22. The filamentary and focusing fields are present irrespective of whether the capsule is of the hot-spot or FI variety.
23. J. Delettrez *et al.*, *Phys. Rev. A* **36**, 3926 (1987).
24. C. Stoeckl *et al.*, *Plasma Phys. Controlled Fusion* **47**, B859 (2005).
25. We thank the OMEGA engineers and operations crew who supported these experiments and General Atomics for providing high-quality backlighter and target capsules. This work was supported by the Fusion Science Center (FSC) at the University of Rochester (grant no. DE-FG03-03NA00058), the National Laser Users Facility (DE-FG52-07NA28059), and the Office of Defense Programs (DE-FG52-06NA26203), all through the U.S. Department of Energy. J.R.R. also acknowledges the FSC for his postdoctoral appointment.

Fig. 5. Circular lineouts of proton fluence obtained from OMEGA shot 46529 at radii of 430 μm (**A**) and 860 μm (**B**). The filamentary structures represent a 2D projection of a 3D field structure that originates inside the critical density surface (**C**).

critical density surface